

Explanation of the nature of the island of inversion exhibited by ^{32}Mg at the Hartree-Fock-Bogoliubov level and beyond*

Yong Peng (彭永)^{1,2} Jia Liu (刘佳)^{1,2#} Jing Geng (耿晶)^{1,2†} Yi Fei Niu (牛一斐)^{1,2,3} Wen Hui Long (龙文辉)^{1,2,3‡}

¹Frontier Science Center for Rare isotope, Lanzhou University, Lanzhou 730000, China

²School of Nuclear Science and Technology, Lanzhou University, Lanzhou 730000, China

³Joint Department for Nuclear Physics, Lanzhou University and Institute of Modern Physics, CAS, Lanzhou 730000, China

Abstract: This work presents an explanation of the nature of the island of inversion exhibited by the unstable nucleus ^{32}Mg , through the applications of the axially deformed relativistic Hartree-Fock-Bogoliubov (D-RHFB) and the configuration-interaction relativistic Hartree-Fock (CI-RHF) models, which correspond to the Hartree-Fock-Bogoliubov level and beyond, respectively. Using the same Lagrangian PKA1, the D-RHFB and CI-RHF models demonstrate an excellent agreement with experimental data for the ground-state deformation and the low-lying excitation energies of ^{32}Mg . Furthermore, a new insight into the nature of the island of inversion is implemented from the breaking of the pseudo-spin symmetry (PSS), in addition to the cross-shell excitation, both of which are essential to give rise to a stable deformation and a rotational collectivity for ^{32}Mg . In particular, the exchange degrees of freedom, like the ρ -tensor coupling in PKA1, are illustrated to play a substantial role in determining the configuration interactions and the binding of the nucleus.

Keywords: Island of inversion, Cross-shell excitation, Pseudo-spin symmetry

DOI: CSTR:

I. INTRODUCTION

The fundamental challenge in the field of nuclear physics is to understand how nucleons interact and combine to form an atomic nucleus. Nuclei far from the stability line, also known as exotic nuclei or unstable nuclei, exhibit a wide range of novel phenomena, including the disappearance of traditional magic shells and the appearance of new (semi-) magic shells [1–9]. The unstable nucleus of interest, namely ^{32}Mg [10, 11], exhibits typical feature of the island of inversion [12–14]. In particular, the experimental evidence, including the large $B(E2 : 2_1^+ \rightarrow 0^+)$ value, the low-lying 2_1^+ excited state and the rotational band [3, 15–21], has established a well-deformed ground state (g.s.) for ^{32}Mg , from which the persistence of a spherical magic shell $N = 20$ is ruled out consistently. All of these findings offer a valuable insight into the mechanisms that govern the binding of nucleus.

In theory, a remarkable cross-shell excitation from neutron sd to pf shells for ^{32}Mg has been proposed for the deformed g.s. 0_1^+ by the shell model with the SDPF-M

interaction [22, 23]. In accordance with the picture of the cross-shell excitation, the intrusion of the pf -shell was frequently observed in the deformed mean-field calculations of ^{32}Mg . Nevertheless, the g.s. deformation remains inadequately described. For instance, the angular momentum projection (AMP) based on the mean-field models is capable of reproducing the deformed g.s. for ^{32}Mg [24–26], but is unable to reproduce the low-lying excitation energies. This indicates that the underlying mechanism responsible for the island of inversion properties exhibited by ^{32}Mg still remains challenging.

As one of the representative nuclear models, the relativistic mean field (RMF) theory [27–34], based on the meson-propagated diagram of nuclear force [35], provides a simple yet efficient modelling of nuclear binding through a covariant representation of the strong attractive scalar and repulsive vector interactions. This picture provides a natural explanation of the strong spin-orbit couplings in nuclei [36, 37] and the origin of pseudo-spin symmetry (PSS) [38, 39]. In particular, as indicated by the conservation conditions, namely $V + S = 0$ [40] or

Received 21 January 2025; Accepted 1 April 2025

* This work is partly supported by the Strategic Priority Research Program of Chinese Academy of Sciences under Grant No. XDB34000000, the Fundamental Research Funds for the Central Universities (Izujbky-2023-stlt01), the National Natural Science Foundation of China under Grant Nos. 12275111 and 12075104, the National Key Research and Development (R&D) Program under Grant No. 2021YFA1601500

† E-mail: gengjing@lzu.edu.cn

‡ E-mail: longwh@lzu.edu.cn

These authors contributed equally as the first authors

©2025 Chinese Physical Society and the Institute of High Energy Physics of the Chinese Academy of Sciences and the Institute of Modern Physics of the Chinese Academy of Sciences and IOP Publishing Ltd. All rights, including for text and data mining, AI training, and similar technologies, are reserved.

$d(V+S)/dr = 0$ [41] with the scalar (S) and vector (V) potentials, the approximate PSS in realistic nuclei is a natural consequence of the relativistic modelling of nuclear binding. However, the Fock terms, an integral part of the meson-propagation diagram, were excluded from the RMF models solely for the sake of simplicity, thereby overlooking the important degrees of freedom associated with the π and ρ -tensor (ρ -T) couplings.

The incorporation of the Fock terms, which account for the exchange correlations, has led to the relativistic Hartree-Fock (RHF) and relativistic Hartree-Fock-Bogoliubov (RHFB) theories [42–45]. With the proposed RHF Lagrangians PKO i ($i = 1, 2, 3$) [43, 46] and PKA1 [44], comparable quantitative precision as the RMF theory has been achieved by the RHF and RHFB theories in describing a range of nuclear phenomena [47]. In order to understand the role of the Fock terms, PKO2, that contains the σ -scalar (σ -S), ω -vector (ω -V) and ρ -vector (ρ -V) couplings, was set to share the same degrees of freedom as popular RMF Lagrangians, PKO1 additionally considers the π -pseudo-vector (π -PV) coupling, which is gradually enhanced in PKO3, and PKA1 further takes into account the ρ -T coupling [automatically the ρ -vector-tensor (ρ -VT) ones], which implements the meson exchange diagram of nuclear force. It is noteworthy that the π -PV and ρ -T couplings contribute almost fully via the Fock terms, which are regarded as the exchange degrees of freedom.

At the early time, it has been established that the Fock terms can significantly enhance the isovector contributions of the energy functional [48]. Practically, the modelling of nuclear binding remains largely unaltered from the RMF models to the PKO series [43, 49], providing a comparable description of the PSS restoration in nuclear structure [50]. However, due to the strong ρ -T coupling, the in-medium balance between nuclear attractive and repulsive interactions, which determines the binding of nucleus, is significantly altered from the popular RMF and PKO models to PKA1 [49]. Consequently, PKA1 correctly restores the PSS for the high- l states, which eliminates the spurious shell closures $N(Z) = 58$ and 92 predicted by the RMF and PKO calculations [44, 49, 51]. The development of new Lagrangians DD-LZ1 [52] and PCF-PK1 [53] was then prompted, with restored PSS for the high- l states and eliminated spurious shell closures.

Recently, both the RHF and RHFB theories have been extended to accommodate axially deformed nuclei, leading to the D-RHF and D-RHFB models [54, 55], respectively. In particular, both the π -PV and ρ -T couplings associated with the exchange correlations have been illustrated to exert a considerable influence on deformed nuclei [54–56]. The D-RHFB model with PKA1 [44] has been demonstrated to reproduce both the even-parity g.s. and halo structure [56], and further to elucidate the coherence between the parity inversion and the halo/cluster

structures in ^{11}Be [57]. More recently, the RHF theory has been extended to include the configuration interactions, leading to the configuration-interaction relativistic Hartree-Fock (CI-RHF) model [58]. It is crucial to highlight that the configuration interactions are constrained by an existing Lagrangian, such as PKA1, in a manner analogous to that employed in Refs. [59–63]. Thus, using the same Lagrangian, a robust methodology for an insight into the g.s. and the low-lying excitations is obtained from the combination of the D-RHFB and CI-RHF models, as well as for the underlying mechanism responsible for the island of inversion properties exhibited by ^{32}Mg .

The paper is organized as follows. In Sec. 2, the CI-RHF model is introduced briefly, with the comments on the relation to the D-RHFB calculations. The low-lying excitation properties and the g.s. deformation of ^{32}Mg are then discussed in Sec. 3, with a special focus on the relation between the breaking of the PSS predicted for spherical ^{32}Mg and the island of inversion properties of ^{32}Mg . At the end, the conclusions and perspectives are given in Sec. 4.

II. CONFIGURATION-INTERACTION RELATIVISTIC HARTREE-FOCK MODEL

In this section, we briefly introduce the CI-RHF model [58]. Similar as the conventional shell model, the CI-RHF calculations are restricted to a truncated Hilbert space, namely the model space, on top of a frozen doubly magic core. Consequently, an effective Hamiltonian is introduced to account for the contributions excluded from the model space. It is noteworthy that the model space is constructed on the single-particle basis given by the spherical RHF calculations, and then the energy of the frozen core is consistently determined.

Starting with a complete set of single-particle basis, the pairing, quadrupole and octupole correlations can be captured through the configuration mixing in a relatively small model space, namely the P -space,

$$P = \sum_n |\Psi_n\rangle\langle\Psi_n|, |\Psi_n\rangle = \prod_{i=1}^{N_{\text{val}}} c_{n_i}^\dagger |\text{core}\rangle, \quad (1)$$

where $|\text{core}\rangle$ represents the frozen core, and the creation operators (c^\dagger) are restricted within the valence space. However, due to the limited model space, an effective Hamiltonian has to be considered to incorporate the important correlations associated with the configurations excluded from the model space. In order to account for the cross-shell excitation, the extended Kuo-Krenciglowa (EKK) method [64, 65] is applied to derive the multi-shell effective Hamiltonian for the CI-RHF calculations,

$$H_l^{\text{eff}} = H^{\text{BH}}(E_0) + \sum_{k=1}^{\infty} \frac{1}{k!} \frac{d^k \hat{Q}(E_0)}{dE_0^k} \{H_{l-1}^{\text{eff}} - E_0\}^k, \quad (2)$$

where the sum on the right side is the folded terms, the index l represents the step of the iterations, and the Bloch-Horowitz Hamiltonian is defined as $H^{\text{BH}}(E) = PH_0P + \hat{Q}(E)$, where H_0 is the unperturbed Hamiltonian. Correspondingly, the effective interaction V^{eff} can be calculated as $V^{\text{eff}} = H^{\text{eff}} - PH_0P$. In practice, the \hat{Q} box is usually approximated as an expansion around H_0 ,

$$\begin{aligned} \hat{Q}(E) &= PVP + PV \frac{Q}{E - H_0} VP \\ &+ PV \frac{Q}{E - H_0} V \frac{Q}{E - H_0} VP + \dots \end{aligned} \quad (3)$$

Obviously the effective Hamiltonian H^{eff} in Eq. (2) is independent of the starting energy E_0 . Therefore, one may tune the value of E_0 to avoid the divergences of energy denominator in the \hat{Q} -box. In the practical calculations of \hat{Q} -box, we only consider the second-order core-polarization corrections to 80 MeV in the single particle energy [58]. Moreover, the folding terms with $k \geq 10$ are terminated in Eq. (2).

Beyond the Hartree-Fock level, the main components of pairing, quadrupole, and even octupole correlations can be naturally included through configuration mixing in the model space. Meanwhile, the correlations associated with high-energy particle-hole excitations, which are excluded from the model space, are incorporated by the effective Hamiltonian. It is thus expected that the CI-RHF model provides reasonable description of the low-lying excitations. In the D-RHFB model, the RHF mean field and pairing correlations are treated within the Bogoliubov scheme in a unified manner [55]. In the intrinsic framework, the quadrupole correlations are taken into account with the presence of quadrupole deformation. This, to a certain extent, indicates some consistency between the D-RHFB and CI-RHF calculations, especially with the same Lagrangian. In particular, the g.s. and low-lying excitations can be well described by the CI-RHF model, whereas the D-RHFB model can provide us an intuitive deformation picture. Consequently, it is imperative to understand the nature of the island of inversion exhibited by ^{32}Mg , through the applications of the CI-RHF and D-RHFB models.

III. RESULTS AND DISCUSSIONS

In this study, the RHF Lagrangian PKO_i ($i = 1, 2, 3$) [43, 46] and PKA1 [44] are utilized in both the D-RHFB and the CI-RHF calculations. In order to provide a more complete understanding, the D-RHFB calculations with

the RMF Lagrangian DD-ME2 [66] and DD-LZ1 [52] are also performed for the nucleus of interest, ^{32}Mg . However, due to the missing of the Fock terms, it is hard to expect that the off-diagonal two-body interaction matrix elements (TBMEs), namely $\bar{V}_{abcd} = V_{abcd} - V_{abdc}$, can be properly evaluated with the RMF Lagrangians, such as DD-ME2 and DD-LZ1, in which the exchange correlations are incorporated phenomenologically by the parameterizations, rather than an explicit treatment. Therefore, the RMF Lagrangians will not be applied in the current CI-RHF calculations.

Within the D-RHFB model, the Bogoliubov quasi-particle orbits, as well as the canonical single-particle ones, are expanded on the spherical Dirac Wood-Saxon (DWS) basis [67], and the details of the space truncations can be found in Ref. [55]. Moreover, the central part of the finite-range Gogny force D1S [68] was utilized as the pairing force in the D-RHFB calculations. For the CI-RHF calculations of ^{32}Mg , the neutron (n) valence orbits include both the sd ($v2s_{1/2}$, $v1d_{3/2}$ and $v1d_{5/2}$) and pf orbits ($v1f_{7/2}$ and $v2p_{3/2}$) in order to account for the cross-shell excitation, and the proton valence space is set as the sd shell, on top of the frozen core ^{16}O .

A. The island of inversion properties of ^{32}Mg

Figure 1 shows the total energies E (MeV) as functions of quadrupole deformation β , given by the shape-constrained D-RHFB calculations. It is observed that PKA1 produces a clear global prolate minimum, displaying a stable deformation for the g.s. of ^{32}Mg . In particular, the deformation given by PKA1 is in a good agreement with

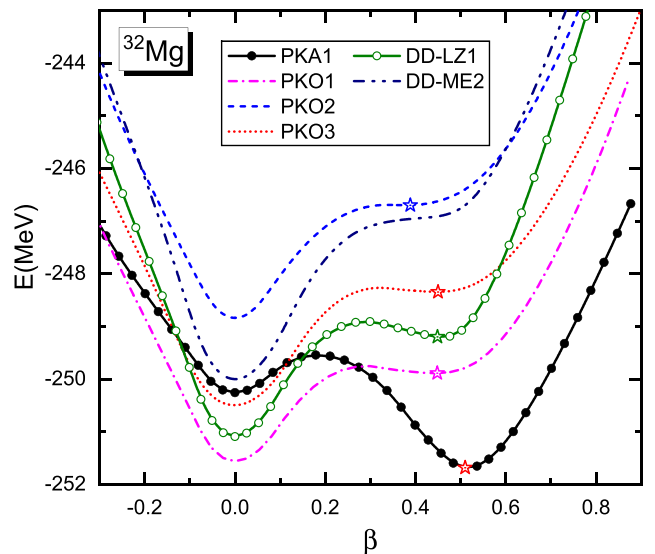


Fig. 1. (Color Online) Total energies E (MeV) of ^{32}Mg as functions of quadrupole deformation β given by the D-RHFB calculations with the RHF Lagrangians PKA1 and PKO_i ($i = 1, 2, 3$), and the RMF ones DD-ME2 and DD-LZ1. The stars denote the prolate minima.

the experimental values of $\beta = 0.512(44)$ [3] and $\beta = 0.51(3)$ [18]. In contrast, all the other selected Lagrangians predict spherical global minima and shoulder-like structure or weak local minimum with prolate deformation. In fact, the deformed calculation with the Lagrangian PCF-PK1 [53] does not support a stable deformation for the g.s. of ^{32}Mg , either. It is also seen in Fig. 1 that the RMF Lagrangian DD-LZ1 [52] present more visible prolate minimum, as compared to the other selected models except PKA1. On the other hand, as indicated by the AMP calculations [24, 26], it is possible to produce a global deformed minimum for ^{32}Mg with these Lagrangians, if further considering the correlations beyond the D-RHFB scheme.

Figure 2 provides us an illustration, by displaying the low-lying excitation spectra and the reduced transition probabilities $B(E2)$ given the CI-RHF calculations with PKA1, PKO2 and PKO3, as compared to the experimental data [15, 19, 69]. The $B(E2)$ values are calculated with the effective charges 1.35 and 0.35 for protons and neutrons, respectively [22]. The results of PKO1 are not shown due to similar description as PKO3. Moreover, Table 1 illustrates the numbers of neutrons populating the valence orbits for the g.s. 0_1^+ . For better understanding, the ratios $R = E(4_1^+)/E(2_1^+)$ are also shown in the last column of Table 1. As illustrated in Fig. 2 and Table 1, the experimental measurements, including the low-lying spectrum, the ratio R and $B(E2 : 2_1^+ \rightarrow 0_1^+)$, indicates a rotational collectivity rather than a vibration one for ^{32}Mg . The low-lying excitation energies and the ratio R given by PKA1 are in an excellent agreement with the experimental data [19, 69]. As referred to the most recently reported value [15], PKA1 overestimates the $B(E2 : 2_1^+ \rightarrow 0_1^+)$ value, but being more consistent with the

earlier measured value 124.4(18.0) $e^2\text{fm}^4$ [21]. In particular, a notable cross-shell excitation is predicted by PKA1 for the g.s. 0_1^+ , with about two neutrons populating the pf shell. It supports a deformed g.s. for ^{32}Mg , being consistent with global prolate minimum given by the PKA1 results in Fig. 1. Consistently, the CI-RHF and D-RHFB calculations with PKA1 yield similar intrinsic electric quadrupole momentums Q^i , reading as 68.9 $e\text{ fm}^2$ and 65.8 $e\text{ fm}^2$, respectively. These results are coincident with the previous shell model calculations [22, 23]. Moreover, PKA1 predicts considerable neutron population on the $2p_{3/2}$ orbit. It is noteworthy that the measured cross section of the g.s. of ^{32}Mg can only be reproduced with a discernible $2p_{3/2}$ contribution [69].

On the other hand, it is seen in Table 1 and Fig. 2 that PKO2 and PKO3 predict not only a notable cross-shell excitation from the sd to the pf shells for the g.s. 0_1^+ , but also fairly large values of $B(E2 : 2_1^+ \rightarrow 0_1^+)$. Specifically, these $B(E2)$ values are consistent with the reported measurements 90.8(15.6) $e^2\text{fm}^4$ [3], 66.6(15.6) $e^2\text{fm}^4$ [16], 89.4(11.4) $e^2\text{fm}^4$ [18] and 86.8(10.4) $e^2\text{fm}^4$ [15], but are smaller than the one 124.4(18.0) $e^2\text{fm}^4$ reported in Ref. [21]. In contrast to the weak local minima in Fig. 1, these results also support a deformed g.s. for ^{32}Mg , after implementing the many-body correlations within the CI-RHF scheme. However, as illustrated in the last column of Table 1, the R -values given by PKO2 and PKO3 are close to the vibration limit 2.0, which indicates near pure vibration collectivity for ^{32}Mg . This is consistent with the calculations of the AMP based on RMF approach [70]. Meanwhile, the low-lying spectra given by PKO2 and PKO3 in Fig. 2 are near equally spaced, representing a typical feature of vibration band. It can be thus deduced that the CI-RHF calculations with both PKO2 and PKO3 predict a soft deformation for ^{32}Mg , which is not as stable as indicated by the measured low-lying excitation spectrum [19].

In order to provide an insight into the g.s. deformation and the collectivity of ^{32}Mg , Table 2 lists the contributions (MeV) of the energy functional, as given by the D-RHFB calculations with PKA1, PKO3 and DD-LZ1, where the first and the second rows for each Lagrangian correspond to the spherical and deformed minima, re-

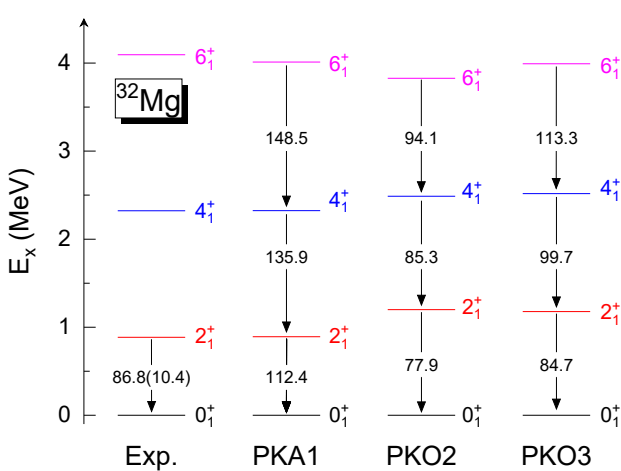


Fig. 2. (Color Online) Low-lying excitation spectra and the reduced transition probabilities $B(E2)$ (in $e^2\text{fm}^4$) values of ^{32}Mg given by the CI-RHF calculations with PKA1, PKO2 and PKO3, in comparison with the experimental data [15, 19, 69].

Table 1. Numbers of neutrons populating the sd and pf orbits for the 0_1^+ state of ^{32}Mg given by the CI-RHF calculations with PKA1, PKO2 and PKO3. The ratio $R = E(4_1^+)/E(2_1^+)$ is also shown in the last column, and the experimental value reads as 2.62 [19, 69].

	$1d_{5/2}$	$2s_{1/2}$	$1d_{3/2}$	$1f_{7/2}$	$2p_{3/2}$	R
PKA1	5.75	1.91	2.27	1.50	0.56	2.61
PKO2	5.73	1.92	2.38	1.81	0.16	2.07
PKO3	5.73	1.92	2.56	1.57	0.23	2.14

Table 2. Contributions (MeV) of the energy functional E , including the kinetic term $E_{\text{kin.}}$, the sum of the isoscalar σ -S and ω -V couplings, the isovector ρ - and π -couplings, and the others $E_{\text{oht.}}$ for the sum of the other channels, namely Coulomb field, pairing correlations and the center-of-mass corrections. The results are given by the D-RHFB calculations with PKA1, PKO3 and DD-LZ1, where the first and the second rows correspond to the spherical and deformed minima, respectively.

	$E_{\text{kin.}}$	$E_{\sigma+\omega}$	E_{ρ}	E_{π}	$E_{\text{oht.}}$	E
PKA1	400.8	-417.0	-217.5	-31.5	14.9	-250.2
	409.6	-434.4	-214.4	-29.9	17.4	-251.7
PKO3	438.1	-606.1	-59.7	-37.2	14.4	-250.5
	448.7	-616.3	-59.2	-36.1	14.6	-248.3
DD-LZ1	412.6	-701.3	18.3	-	19.4	-251.1
	414.1	-702.7	17.6	-	21.8	-249.2

spectively. It is obvious that the total bindings described by PKA1, PKO3 and DD-LZ1 are not much different for ^{32}Mg . As illustrated in Table 2, the modelling of nuclear binding remains largely unaltered from DD-LZ1 to PKO3, although the isovector contributions in PKO3 are enhanced by the Fock terms. However, the contributions of the ρ -couplings in PKA1, due to the ρ -T and ρ -VT couplings, become competitive with the interplay of the strong attractive σ -S and repulsive ω -V couplings. It is noteworthy that the E_{ρ} term described by PKA1 is reduced from the spherical to the deformed cases, whereas the $E_{\sigma+\omega}$ term is much enhanced, leading to the deformed g.s. for ^{32}Mg . This reveals that the modelling of nuclear binding undergoes a significant alteration with the presence of the Fock terms, especially for the exchange degrees of freedom associated with the ρ -T and ρ -VT couplings.

As an extensive illustration beyond the Hartree-Fock-Bogoliubov level, Fig. 3 displays the main sd -to- pf cross-shell matrix elements, as given by PKA1 (left pillars), PKO3 (middle pillars) and PKO2 (right pillars). The contributions from the exchange degrees of freedom, namely the ρ -T (automatically including the ρ -VT one) and π -PV couplings, are indicated by the patterns, and the black color represents the sum of the dominant channels (d.c.), which includes the degrees of freedom considered in the popular RMF models and PKO2, namely the σ -S, ω -V and ρ -V couplings. In particular, the black bars overlapped with the red patterns indicate the cancellations between the d.c. and the ρ -T coupling, and the lengthy of the pillars, after the cancellations, represents the total results.

As shown in Fig. 3, the configuration interactions given by PKA1 are predominantly shaped by the ρ -T coupling. Moreover, the π -PV coupling also makes discernible contributions, despite its relatively weak coupling strength [44, 46]. With the presence of the π -PV coupling, the d.c. contributions are slightly changed from PKO2 to PKO3, but notably reduced for the cases $(ff\text{d}^5\text{d}^5)_{J=0}$ and $(ff\text{d}^5\text{d}^5)_{J=2}$. This indicates the signifi-

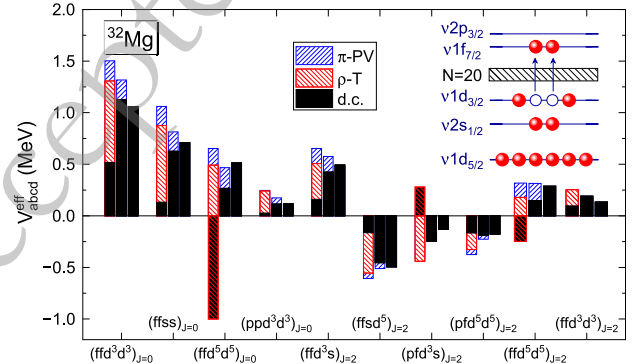


Fig. 3. (Color Online) Schematic of the cross-shell excitation and the main sd -to- pf cross-shell matrix elements given by PKA1 (left pillars), PKO3 (middle pillars) and PKO2 (right pillars), where f , p , s , d^3 and d^5 represent the neutron orbits $1f_{7/2}$, $2p_{3/2}$, $2s_{1/2}$, $1d_{3/2}$ and $1d_{5/2}$, respectively. The dominant channel (d.c.) contains the σ -S, ω -V and ρ -V couplings.

ance of the π -PV coupling in determining some configuration interactions. Further for PKA1, which incorporates the ρ -T and ρ -VT couplings, the contributions of the d.c. are remarkably changed from PKO3 for most cases. This is consistent with the underlying alteration of the nuclear binding in Table 2, where the sum of the dominant σ -S and ω -V contributions is reduced significantly from PKO3 to PKA1. In particular for the cases $(ff\text{d}^5\text{d}^5)_{J=0}$, $(ff\text{d}^3\text{d}^5)_{J=2}$ and $(ff\text{d}^5\text{d}^5)_{J=2}$, notable cancellations appear between the contributions from the d.c., and the ρ -T and π -PV couplings. This indicates that the exchange degrees of freedom associated with the π -PV and ρ -T couplings can exert an even more important effects in determining the configuration interactions, in comparison to the modelling of nuclear binding at the Hartree-Fock-Bogoliubov level as illustrated in Table 2. Further, this also demonstrates the significance of the Fock terms, especially the exchange degrees of freedom that are absent at the Hartree level.

As discussed above, the exchange degrees of freedom play a substantial role in determining both the nuclear binding and the configuration interactions. However, it

is still not so straightforward to understand why PKA1 predicts a stable deformation and consistent collectivity with the experimental measurements, whereas the PKO models prefer a near pure vibration collectivity with soft quadrupole deformation for ^{32}Mg . This calls for a further investigation on the microscopic single-particle structure given by the D-RHFB calculations.

B. Microscopic understanding of the deformation in ^{32}Mg

In light of the results in [Table 1](#), the cross-shell excitation supports the occurrence of the deformation for the g.s. of ^{32}Mg under the CI-RHF scheme. Among the selected Lagrangians, PKA1 achieves an excellent agreement with the experimental data for both the deformation and the low-lying excitation energies. In contrast, regarding the ratio $R = E(4_1^+)/E(2_1^+)$ in [Table 1](#) and the low-lying spectra in [Fig. 2](#), PKO2 and PKO3 predict a vibration band for ^{32}Mg . In order to better understand the nature of the island of inversion exhibited by ^{32}Mg , [Fig. 4](#) shows the evolution of neutron canonical single-particle orbits with respect to the deformation β . The results are extracted from the D-RHFB calculations with PKA1 (solid lines) and PKO3 (dashed lines), the representatives of the selected models.

As illustrated in [Fig. 4](#), the intrusion of the pf shell, namely the $1/2_3^-$ orbit, is observed in both the PKO3 and

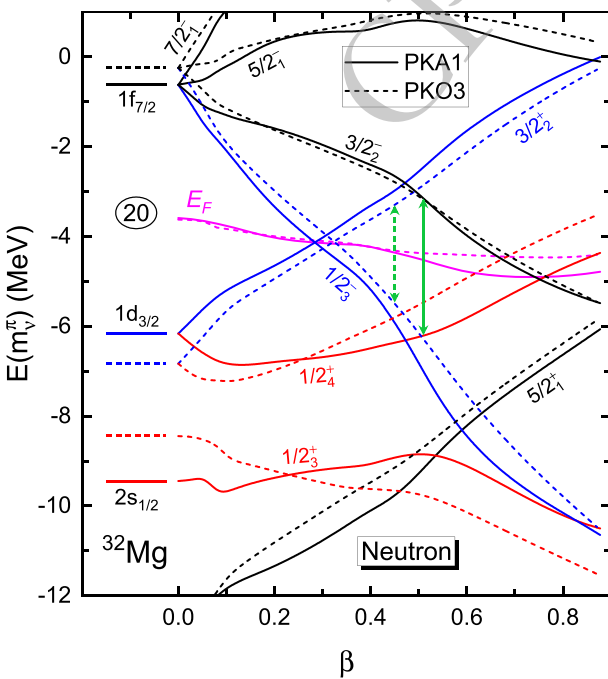


Fig. 4. (Color Online) Neutron canonical single-particle energies of ^{32}Mg as functions of the deformation β , as given by PKA1 (solid lines) and PKO3 (dotted lines). The arrows mark the shell gap at the prolate minima ($\beta = 0.51$ for PKA1 and 0.45 for PKO3).

PKA1 results. This intrusion is consistent with the sd -to- pf cross-shell excitation given by the spherical CI-RHF calculations in [Table 1](#). Moreover, due to smaller spherical shell gap of $N = 20$, an accelerated intrusion of the $1/2_3^-$ orbit is predicted by PKA1 than by PKO3, which results in earlier intersection of the orbits $1/2_3^-$ and $3/2_2^+$. This, to a certain extent, is meaningful for the occurrence of a stable deformation in ^{32}Mg . More significantly, PKA1 presents much flatter shape evolution than PKO3 for both the orbits $1/2_3^+$ and $1/2_4^+$, which branch from the pseudo-spin (PS) partners $2s_{1/2}$ and $1d_{3/2}$. In particular, the $1/2_4^+$ orbit described by PKA1 remains more deeply bound than the spherical $1d_{3/2}$ state before reaching the global minimum. As a result, PKA1 produces a more notable shell gap (marked in arrows) at the prolate minimum than PKO3. Although much less pronounced than the spherical one $N = 20$, this notable shell gap is still essential for stabilizing the g.s. deformation of ^{32}Mg . Accordingly, as illustrated by the PKA1 results in [Fig. 1](#), the energy of the system is predicted to increase rapidly when the deformation deviates from the prolate minimum. This explains why the nucleus ^{32}Mg described by PKA1 exhibits the rotational rather than the vibrational collectivity, being consistent with the low-lying spectra in [Fig. 2](#).

In order to provide a deep understanding for the occurrence of a stable deformation in ^{32}Mg , [Fig. 5a](#) displays the quadrupole moment Q_2 (fm^2) as a function of the deformation β for both neutron orbits $1/2_3^+$ and $1/2_4^+$, and [Fig. 5b](#) for the proportions of main spherical DWS waves in the orbit $1/2_4^+$. It is known well that the mixture of spherical waves subsequent to the deformation is sensitive to the presence of a spherical shell gap. As illustrated in the left of [Fig. 4](#), PKA1 yields much more distinct splitting between the spherical PS partners ($1d_{3/2}$, $2s_{1/2}$) than PKO3, thereby illustrating a notable breaking of the PSS. Consequently, as illustrated in [Fig. 5b](#), this prevents the mixture of the $2s_{1/2}$ wave into the $1/2_4^+$ orbit as described by PKA1. Similarly, less mixture of the $1d_{3/2}$ wave into the $1/2_3^+$ orbit is predicted by PKA1 than by PKO3. Consistently, the Q_2 values given by PKA1 and PKO3 differ significantly for both the $1/2_3^+$ and $1/2_4^+$ orbits as illustrated in [Fig. 5a](#).

Combined with the Q_2 values in [Fig. 5a](#), the shape evolutions of the $1/2_3^+$ and $1/2_4^+$ orbits in [Fig. 4](#) are easily understood. As deduced from the Q_2 values in [Fig. 5a](#), PKO3 predicts the $1/2_4^+$ orbit exhibiting oblate distribution, which thus becomes less and less bound when the nucleus ^{32}Mg is more and more prolately deformed, and vice versa for the $1/2_3^+$ orbit. However, both the $1/2_3^+$ and $1/2_4^+$ orbits described by PKA1 exhibit near spherical nature before reaching the prolate minimum. Consistently, as illustrated in [Fig. 4](#), both the $1/2_3^+$ and $1/2_4^+$ orbits described by PKA1 exhibit much flattened shape evolutions. In fact, the flat evolution of the $1/2_4^+$ orbit is essential for giving rise to the distinct deformed shell gap

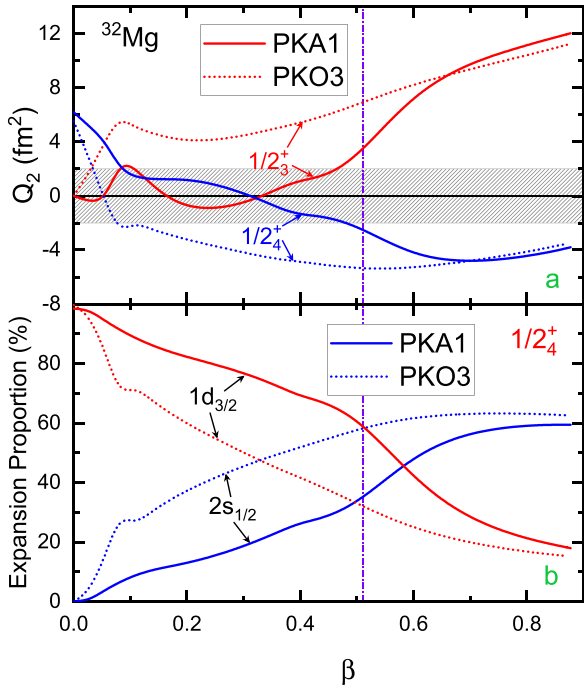


Fig. 5. (Color Online) Quadrupole moment Q_2 (fm 2) for neutron orbits $1/2_3^+$ and $1/2_4^+$ (plot a) and the proportions (in percentage) of main spherical DWS waves in the orbit $1/2_4^+$ of ^{32}Mg , as given by PKA1 (solid lines) and PKO3 (dotted lines).

and further the stable deformation in ^{32}Mg .

As previously stated, the cross-shell excitation or the pf intrusion is essential for the occurrence of a deformation in ^{32}Mg . In addition to that, the stability of the deformation, which plays a crucial role in determining the collectivity of ^{32}Mg , is intrinsically connected with the PSS breaking between neutron spherical PS partners ($2s_{1/2}, 1d_{3/2}$). A new insight into the nature of the island of inversion exhibited by ^{32}Mg is thus implemented from the PSS breaking, which is a consequence of nuclear binding as indicated by the PSS conditions [40, 41]. Moreover, as illustrated in Table 2 and Fig. 3, the ρ -T couplings play a substantial role in determining both the nuclear binding and the configuration interactions. This also reveals the role of the exchange degrees freedom in determining the island of inversion properties of ^{32}Mg .

On the other hand, the Lagrangians PCF-PK1 and DD-LZ1 can properly restore the PSS for the high- l states as PKA1 [52, 53]. However, PCF-PK1, as well as DD-

ME2, PKO1 and PKO2, presents similar description on the splitting of the PS partners ($1d_{3/2}, 2s_{1/2}$) and the $N = 20$ shell in spherical ^{32}Mg . It is thus not much expected that PCF-PK1 provides equivalent description as PKA1 for the nucleus of interest, ^{32}Mg . In contrast, similar as PKA1, DD-LZ1 produces notable PSS breaking and flat shape evolutions for the deformed orbits $1/2_3^+$ and $1/2_4^+$. While, as aforementioned, it is not a proper choice to use the RMF Lagrangian DD-LZ1 to derive an effective Hamiltonian for the CI-RHF calculations.

IV. CONCLUSIONS

In conclusion, the nature of the island of inversion exhibited by the unstable nucleus ^{32}Mg , namely a well-deformed ground state with vanishing neutron shell $N = 20$, has been investigated through the applications of the axially deformed relativistic Hartree-Fock-Bogoliubov (D-RHFB) and the configuration-interaction relativistic Hartree-Fock (CI-RHF) models. Using the same Lagrangian PKA1, the D-RHFB and CI-RHF models well reproduce the stable deformation and the low-lying excitations of ^{32}Mg at the Hartree-Fock-Bogoliubov level and beyond, respectively. In addition to the picture of the pf intrusion or the cross-shell excitation, a new insight into the occurrence of a stable deformation in ^{32}Mg is implemented from the breaking of the pseudo-spin symmetry (PSS). It is found that due to the notable PSS breaking, a notable deformed shell gap is predicted by PKA1, which stabilizes the deformation of ^{32}Mg and gives rise to the rotational collectivity as revealed by the experimental measurements.

In particular, it is illustrated that the degrees of freedom associated with the exchange correlations, especially the ρ -tensor coupling, present significant contributions to the nuclear binding and the configuration interactions, which are essential in giving rise to the PSS breaking and the cross-shell excitation for ^{32}Mg , respectively. This reveals the significance of exchange correlations in understanding the nature of the island of inversion, as well as for the binding of nucleus, a fundamental issue in the field of nuclear physics. At the end, it is worthwhile to comment that the CI-RHF calculation with PKA1 yields similar excitation energy $E(0_2^+)$ as the shell model calculations with the SDPF-M interaction [22, 23], which deserves an extensive study in future.

References

- [1] C. R. Hoffman, T. Baumann, D. Bazin, J. Brown, G. Christian, P. A. DeYoung, J. E. Finck, N. Frank, J. Hinnefeld, R. Howes, P. Mears, E. Mosby, S. Mosby, J. Reith, B. Rizzo, W. F. Rogers, G. Peaslee, W. A. Peters, A. Schiller, M. J. Scott, S. L. Tabor, M. Thoennessen, P. J. Voss, and T. Williams, *Phys. Rev. Lett.* **100**, 152502 (2008)
- [2] H. Simon, D. Aleksandrov, T. Aumann, L. Axelsson, T. Baumann, M. J. G. Borge, L. V. Chulkov, R. Collatz, J. Cub, W. Dostal, B. Eberlein, Th. W. Elze, H. Emling, H. Geissel, A. Grünschloss, M. Hellström, J. Holeczek, R. Holzmann, B. Jonson, J. V. Kratz, G. Kraus, R. Kulessa, Y. Leifels, A. Leistenschneider, T. Leth, I. Mukha, G. Münenberg, F. Nickel, T. Nilsson, G. Nyman, B. Petersen,

- M. Pfützner, A. Richter, K. Riisager, C. Scheidenberger, G. Schrieder, W. Schwab, M. H. Smedberg, J. Stroth, A. Surowiec, O. Tengblad, and M. V. Zhukov, *Phys. Rev. Lett.* **83**, 496 (1999)
- [3] T. Motobayashi, Y. Ikeda, Y. Ando, K. Ieki, M. Inoue, N. Iwasa, T. Kikuchi, M. Kurokawaa, S. Moriya, S. Ogawa, H. Murakamia, S. Shimouraa, Y. Yanagisawa, T. Nakamura, Y. Watanabe, M. Ishihara, T. Teranishi, H. Okuno, and R. F. Casten, *Phys. Lett. B* **346**, 9 (1995)
- [4] K. Tshoo, Y. Satou, H. Bhang, S. Choi, T. Nakamura, Y. Kondo, S. Deguchi, Y. Kawada, N. Kobayashi, Y. Nakayama, K. N. Tanaka, N. Tanaka, N. Aoi, M. Ishihara, T. Motobayashi, H. Otsu, H. Sakurai, S. Takeuchi, Y. Togano, K. Yoneda, Z. H. Li, F. Delaunay, J. Gibelin, F. M. Marqués, N. A. Orr, T. Honda, M. Matsushita, T. Kobayashi, Y. Miyashita, T. Sumikama, K. Yoshinaga, S. Shimoura, D. Sohler, T. Zheng, and Z. X. Cao, *Phys. Rev. Lett.* **109**, 022501 (2012)
- [5] A. Ozawa, T. Kobayashi, T. Suzuki, and K. Yoshidaand I. Tanihata, *Phys. Rev. Lett.* **84**, 5493 (2000)
- [6] R. Kanungo, C. Nociforo, A. Prochazka, T. Aumann, D. Boutin, D. Cortina-Gil, B. Davids, M. Diakaki, F. Farinon, H. Geissel, R. Gernhäuser, J. Gerl, R. Janik, B. Jonson, B. Kindler, R. Knöbel, R. Krücken, M. Lantz, H. Lenske, Y. Litvinov, B. Lommel, K. Mahata, P. Maierbeck, A. Musumarra, T. Nilsson, T. Otsuka, C. Perro, C. Scheidenberger, B. Sitar, P. Strmen, B. Sun, I. Szarka, I. Tanihata, Y. Utsuno, H. Weick, and M. Winkler, *Phys. Rev. Lett.* **102**, 152501 (2009)
- [7] A. Gade, R. V. F. Janssens, D. Bazin, R. Broda, B. A. Brown, C. M. Campbell, M. P. Carpenter, J. M. Cook, A. N. Deacon, D.-C. Dinca, B. Fornal, S. J. Freeman, T. Glasmacher, P. G. Hansen, B. P. Kay, P. F. Mantica, W. F. Mueller, J. R. Terry, J. A. Tostevin, and S. Zhu, *Phys. Rev. C* **74**, 021302 (2006)
- [8] D. Steffenbeck, S. Takeuchi, N. Aoi, P. Doornenbal, M. Matsushita, H. Wang, Y. Utsuno, H. Baba, S. Go, J. Lee, K. Matsui, S. Michimasa, T. Motobayashi, D. Nishimura, T. Otsuka, H. Sakurai, Y. Shiga, N. Shimizu, P.-A. Söderström, T. Sumikama, R. Taniuchi, J. J. Valiente-Dobón, and K. Yoneda, *Phys. Rev. Lett.* **114**, 252501 (2015)
- [9] D. Steffenbeck, S. Takeuchi, N. Aoi, P. Doornenbal, M. Matsushita, H. Wang, H. Baba, N. Fukuda, S. Go, M. Honma, J. Lee, K. Matsui, S. Michimasa, T. Motobayashi, D. Nishimura, T. Otsuka, H. Sakurai, Y. Shiga, P.-A. Söderström, T. Sumikama, H. Suzuki, R. Taniuchi, Y. Utsuno, J. J. Valiente-Dobón, and K. Yoneda, *Nature* **502**, 207 (2013)
- [10] E. Caurier, G. Martínez-Pinedo, F. Nowacki, A. Poves, and A. P. Zuker, *Rev. Mod. Phys.* **77**, 427 (2005)
- [11] O. Sorlin and M.-G. Porquet, *Prog. Part. Nucl. Phys.* **61**, 602 (2008)
- [12] S. M. Lenzi, F. Nowacki, A. Poves, and K. Sieja, *Phys. Rev. C* **82**, 054301 (2010)
- [13] H. L. Crawford, P. Fallon, A. O. Macchiavelli, P. Doornenbal, N. Aoi, F. Browne, C. M. Campbell, S. Chen, R. M. Clark, M. L. Cortés, M. Cromaz, E. Ideguchi, M. D. Jones, R. Kanungo, M. MacCormick, S. Momiyama, I. Murray, M. Niikura, S. Paschalidis, M. Petri, H. Sakurai, M. Salathe, P. Schrock, D. Steffenbeck, S. Takeuchi, Y. K. Tanaka, R. Taniuchi, H. Wang, and K. Wimmer, *Phys. Rev. Lett.* **122**, 052501 (2019)
- [14] D. S. Ahn, N. Fukuda, H. Geissel, N. Inabe, N. Iwasa, T. Kubo, K. Kusaka, D. J. Morrissey, D. Murai, T. Nakamura, M. Ohtake, H. Otsu, H. Sato, B. M. Sherrill, Y. Shimizu, H. Suzuki, H. Takeda, O. B. Tarasov, H. Ueno, Y. Yanagisawa, and K. Yoshida, *Phys. Rev. Lett.* **123**, 212501 (2019)
- [15] B. Pritychenko, M. Birch, B. Singh, and M. Horoi, *Atomic Data and Nuclear Data Tables* **107**, 1 (2016)
- [16] B.V. Pritychenko, T. Glasmacher, P.D. Cottle, M. Fauerbach, R.W. Ibbotson, K.W. Kemper, V. Maddalena, A. Navin, R. Ronningen, A. Sakharuk, H. Scheit, and V.G. Zelevinsky, *Phys. Lett. B* **461**, 322 (1999)
- [17] D. Guillemaud-Mueller, C. Detraz, M. Langevin, F. Naulin, M. DE Saint-Simon, C. Thibault, F. Touchard, and M. Epherre, *Nucl. Phys. A* **426**, 37 (1984)
- [18] J. A. Church, C. M. Campbell, D.-C. Dinca, J. Enders, A. Gade, T. Glasmacher, Z. Hu, R. V. F. Janssens, W. F. Mueller, H. Olliver, B. C. Perry, L. A. Riley, and K. L. Yurkewicz, *Phys. Rev. C* **72**, 054320 (2005)
- [19] S. Takeuchi, N. Aoi, T. Motobayashi, S. Ota, E. Takeshita, H. Suzuki, H. Baba, T. Fukui, Y. Hashimoto, K. Ieki, N. Imai, H. Iwasaki, S. Kanno, Y. Kondo, T. Kubo, K. Kurita, T. Minemura, T. Nakabayashi, T. Nakamura, T. Okumura, T. K. Onishi, H. Sakurai, S. Shimura, R. Sugou, D. Suzuki, M. K. Suzuki, M. Takashina, M. Tamaki, K. Tanaka, Y. Togano, and K. Yamada, *Phys. Rev. C* **79**, 054319 (2009)
- [20] H. L. Crawford, P. Fallon, A. O. Macchiavelli, A. Poves, V. M. Bader, D. Bazin, M. Bowry, C. M. Campbell, M. P. Carpenter, R. M. Clark, M. Cromaz, A. Gade, E. Ideguchi, H. Iwasaki, C. Langer, I. Y. Lee, C. Loelius, E. Lunderberg, C. Morse, A. L. Richard, J. Rissanen, D. Smalley, S. R. Stroberg, D. Weisshaar, K. Whitmore, A. Wiens, S. J. Williams, K. Wimmer, and T. Yamamoto, *Phys. Rev. C* **93**, 031303(R) (2016)
- [21] V. Chiste, A. Gillibert, A. Lepine Szily, N. Alamanos, F. Auger, J. Barrette, F. Braga, M. D. Cortina Gil, Z. Dlouhy, V. Lapoux, M. Lewitowicz, R. Lichtenhaler, R. Liguori Neto, S. M. Lukyanov, M. MacCormick, F. Marie, W. Mittig, F. de Oliveira Santos, N.A. Orr, A. N. Ostrowski, S. Ottini, A. Pakou, Yu. E. Penionzhkevich, P. Roussel-Chomaz, and J. L. Sida, *Phys. Lett. B* **514**, 233 (2001)
- [22] E. Caurier, F. Nowacki, and A. Poves, *Phys. Rev. C* **90**, 014302 (2014)
- [23] N.Kitamura, K.Wimmer, A.Poves, N.Shimizu, J.A.Tostevin, V.M.Bader, C.Bancroft, D.Barofsky, T.Baugher, D.Bazin, J.S.Berryman, V.Bildstein, A.Gade, N.Imai, T.Kroll, C.Langer, J.Lloyd, E.Lunderberg, F.Nowacki, G.Perdikakis, F.Recchia, T.Redpath, S.Saenz, D.Smalley, S.R.Stroberge, Y.Utsuno, D.Weisshaar, and A.Westerberg, *Phys. Lett. B* **822**, 136682 (2021)
- [24] R. Rodríguez-Guzmán, J.L. Egido, and L.M. Robledo, *Nucl. Phys. A* **709**, 201 (2002)
- [25] J. M. Yao, J. Meng, P. Ring, and D. Pena Arteaga, *Phys. Rev. C* **79**, 044312 (2009)
- [26] Nuria López Vaquero, J. Luis Egido, and Tomás R. Rodíguez, *Phys. Rev. C* **88**, 064311 (2013)
- [27] Brian D. Serot and J. D. Walecka, *Adv. Nucl. Phys.* **16**, 1 (1986)
- [28] P-G. Reinhard, *Rep. Prog. Phys.* **52**, 439 (1989)
- [29] Peter Ring, *Prog. Part. Nucl. Phys.* **37**, 193 (1996)
- [30] Michael Bender, Paul-Henri Heenen, and Paul-Gerhard Reinhard, *Revs. Mod. Phys.* **75**, 121 (2003)
- [31] D. Vretenar, A. V. Afanasjev, G. A. Lalazissis, and P. Ring,

- Phys. Rep.** **409**, 101 (2005)
- [32] Jie Meng, H. Toki, S. G. Zhou, S. Q. Zhang, Wen Hui Long, and L. S. Geng, **Prog. Part. Nucl. Phys.** **57**, 470 (2006)
- [33] T. Nikšić, D. Vretenar, and P. Ring, **Prog. Part. Nucl. Phys.** **66**, 519 (2011)
- [34] Haozhao Liang, Jie Meng, and Shan-Gui Zhou, **Phys. Rep.** **570**, 1 (2015)
- [35] H. Yukawa, Proc. Phys. Math. Soc. Japan **17**, 48 (1935)
- [36] Maria G. Mayer, **Phys. Rev.** **74**, 235 (1948)
- [37] M. G. Mayer, **Phys. Rev.** **75**, 1969 (1949)
- [38] A. Arima, M. Harvey, and K. Shimizu, **Phys. Lett. B** **30**, 517 (1969)
- [39] K. T. Hecht and A. Adler, **Nucl. Phys. A** **137**, 129 (1969)
- [40] Joseph N. Ginocchio, **Phys. Rev. Lett.** **78**, 436 (1997)
- [41] J. Meng, K. Sugawara-Tanabe, S. Yamaji, P. Ring, and A. Arima, **Phys. Rev. C** **58**, R628 (1998)
- [42] A. Bouyssy, J. F. Mathiot, N. Van Giai, and S. Marcos, **Phys. Rev. C** **36**, 380 (1987)
- [43] Wen Hui Long, Nguyen Van Giai, and Jie Meng, **Phys. Lett. B** **640**, 150 (2006)
- [44] Wen Hui Long, Hiroyuki Sagawa, Nguyen Van Giai, and Jie Meng, **Phys. Rev. C** **76**, 034314 (2007)
- [45] Wen Hui Long, Peter Ring, Nguyen Van Giai, and Jie Meng, **Phys. Rev. C** **81**, 024308 (2010)
- [46] Wen Hui Long, Hiroyuki Sagawa, Jie Meng, and Nguyeng Van Giai, **Europhys. Lett.** **82**, 12001 (2008)
- [47] Shihang Shen, Haozhao Liang, Wen Hui Long, Jie Meng, and Peter Ring, **Prog. Part. Nucl. Phys.** **109**, 103713 (2019)
- [48] A. Bouyssy, S. Marcos, J. F. Mathiot, and Nguyen Van Giai, **Phys. Rev. Lett.** **55**, 1731 (1985)
- [49] Jing Geng, Jia Jie Li, Wen Hui Long, Yi Fei Niu, and Shi Yao Chang, **Phys. Rev. C** **100**, 051301(R) (2019)
- [50] Wen Hui Long, Hiroyuki Sagawa, Jie Meng, and Nguyen Van Giai, **Phys. Lett. B** **639**, 242 (2006)
- [51] Li Sheng Geng, Jie Meng, Toki Hiroshi, Wen Hui Long, and Gang Shen, **Chin. Phys. Lett.** **23**, 1139 (2006)
- [52] Bin Wei, Qiang Zhao, Zhi-Heng Wang, Jing Geng, Bao-Yuan Sun, Yi-Fei Niu, and Wen-Hui Long, **Chin. Phys. C** **44**, 074107 (2020)
- [53] Qiang Zhao, Zheng xue Ren, Peng wei Zhao,, and Jie Meng, **Phys. Rev. C** 106 (2022)
- [54] Jing Geng, Jian Xiang, Bao Yuan Sun, and Wen Hui Long, **Phys. Rev. C** **101**, 064302 (2020)
- [55] Jing Geng and Wen Hui Long, **Phys. Rev. C** **105**, 034329 (2022)
- [56] Jing Geng, Yi Fei Niu, and Wen Hui Long, **Chin. Phys. C** **47**, 044102 (2023)
- [57] Jing Geng, Peng Wei Zhao, Yi Fei Niu, and Wen Hui Long, **Phys. Lett. B** **858**, 139036 (2024)
- [58] Jia Liu, Yi Fei Niu, and Wen Hui Long. Confuration interaction relativistic hartree-fock model. *arXiv: 2411.05370*, 2024.
- [59] M. Waroquier, G. Wenés, and K. Heyde, **Nucl. Phys. A** **404**, 298 (1983)
- [60] E. Bender, K.W. Schmid, and Amand Faessler, **Nucl. Phys. A** **596**, 1 (1996)
- [61] B. Alex Brown, Angelo Signoracci, and Morten Hjorth-Jensen, **Phys. Lett. B** **695**, 507 (2011)
- [62] P. W. Zhao, P. Ring,, and J. Meng, **Phys. Rev. C** **94**, 041301(R) (2016)
- [63] W. G. Jiang, B. S. Hu, Z. H. Sun, and F. R. Xu, **Phys. Rev. C** **98**, 044320 (2018)
- [64] Kazuo Takayanagi, **Nucl. Phys. A** **852**, 61 (2011)
- [65] Naofumi Tsunoda, Kazuo Takayanagi, Morten Hjorth-Jensen, and Takaharu Otsuka, **Phys. Rev. C** **89**, 024313 (2014)
- [66] G. A. Lalazissis, T. Nikšić, D. Vretenar, and P. Ring, **Phys. Rev. C** **71**, 024312 (2005)
- [67] Shan-Gui Zhou, Jie Meng, and Peter Ring, **Phys. Rev. C** **68**, 034323 (2003)
- [68] J. F. Berger, M. Girod, and D. Gogny, **Nucl. Phys. A** **428**, 23 (1984)
- [69] K. Wimmer, T. Kröll, R. Krüken, V. Bildstein, R. Gernhäuser, B. Bastin, N. Bree, J. Diriken, P. Van Duppen, M. Huyse, N. Patronis, P. Vermaelen, D. Voulot, J. Van de Walle, F. Wenander, L. M. Fraile, R. Chapman, B. Hadinia, R. Orlandi, J. F. Smith, R. Lutter, P. G. Thirolf, M. Labiche, A. Blazhev, M. Kalküler, P. Reiter, M. Seidlitz, N. Warr, A. O. Macchiavelli, H. B. Jeppesen, E. Fiori, G. Georgiev, G. Schrieder, S. Das Gupta, G. Lo Bianco, S. Nardelli, J. Butterworth, J. Johansen,, and K. Riisager, **Phys. Rev. Lett.** **105**, 252501 (2010)
- [70] J. M. Yao, H. Mei, H. Chen, J. Meng, P. Ring,, and D. Vretenar, **Phys. Rev. C** **83**, 014308 (2011)